Journal of Molecular Structure: THEOCHEM 946 (2010) 57–64

Contents lists available at ScienceDirect

Journal of Molecular Structure: THEOCHEM

journal homepage: www.elsevier.com/locate/theochem

Atomic-scale insight into the oxygen ionic transport mechanisms in La_2NiO_4-based materials

E.N. Naumovich *, V.V. Kharton

Department of Ceramics and Glass Engineering, CICECO, University of Aveiro, 3810-193 Aveiro, Portugal

ARTICLE INFO

Article history:
Received 20 July 2009
Received in revised form 29 September 2009
Accepted 3 December 2009
Available online 4 January 2010

Keywords:
Molecular dynamics
Atomistic computer simulations
Ionic conduction
Lanthanum nickelate
Ruddlesden-Popper family
K_2NiF_4-type compounds

ABSTRACT

The computer simulation studies employing both static lattice and molecular dynamics (MD) methods, were used to identify anion migration pathways, relevant energetic parameters and effects of the transition metal cation dopants on oxygen ion transport in $La_2Ni(M)O_{4+\delta}$ (M = Fe, Co, Cu) solid solutions, a family of promising oxide materials for fuel cell electrodes and dense ceramic membranes for oxygen separation. The factors related to different oxygen sublattices in the K_2NiF_4-type structure of $La_2Ni(M)O_{4+\delta}$ were appraised analyzing the MD data. The results show, in particular, that the incorporation of dopants having 3+ oxidation state leads to higher ionic charge-carrier concentration affecting the overall anion diffusivity, which is essentially determined by cooperative mechanisms involving oxygen interstitials and anions occupying regular apical sites in the layered lattices. However, these dopants tend to decrease anion mobility, both in the rock-salt and perovskite-like layers of the K_2NiF_4-type structure. The likely microscopic mechanisms of anion diffusion in oxygen-hyperstoichiometric $La_2Ni(M)O_{4+\delta}$ are determined.

© 2009 Elsevier B.V. All rights reserved.

1. Introduction

Oxide materials with mixed oxygen-ionic and electronic conductivity have numerous promising applications, such as dense ceramic membranes for oxygen separation and partial oxidation of light hydrocarbons, fuel cell electrodes, sensors and electrocatalytic reactors. An attractive combination of properties important for these applications, namely a relatively high mixed conductivity, moderate thermal expansion and dimensional stability, is known for the Ruddlesden-Popper (RP) type nickelates, in particular for $La_2NiO_{4+\delta}$ and its derivatives with the K_2NiF_4 structure [1–4]. The intergrowth RP structures are built of alternating perovskite-like and rock-salt layers, where oxygen anions can diffuse via the vacancy and interstitial migration mechanisms, respectively. Whilst two-dimensional electronic transport occurs predominantly in the perovskite sheets containing transition metal cations, the rock-salt type blocks govern thermomechanical stability and, often, oxygen interstitial migration [1,2,5,6]. For the compounds with K_2NiF_4 type structure where the number of rock-salt layers is maximum with respect to other members of the RP family, the role of mobile interstitials may become critically important [1,2,7,8]. Information on the microscopic anion-diffusion mechanisms in the RP type compounds is still scarce, a result of their structural complexity and sophisticated defect chemistry.

This work is focused on the computer simulations of ionic transport in the end members of the RP nickelate family, La_2NiO_4-based solid solutions, using the molecular dynamics (MD) and static-lattice simulation (SLS) methods. The experimental results, used in the present work for the sake of comparative analysis and for the defect model formulation, were summarized in previous publications ([9,10] and references cited).

2. Structure, defects and modeling techniques

La_2NiO_4-based solid solutions possess a K_2NiF_4 type structure, schematically shown in Fig. 1. When the oxygen excess is moderate, close to the typical values under application conditions in atmospheric air and at elevated temperatures, this structure has tetragonal symmetry (space group *I4/mmm*); a number of orthorhombic modifications may form at relatively low and high values of the oxygen hyperstoichiometry, δ [11–13]. $La_2NiO_{4+\delta}$ is the first member of the Ruddlesden-Popper series $(LaO)(LaNiO_3)_n$, with $n = 1$. The rock-salt La_2O_2 sheets may accommodate a significant oxygen excess charge-compensated by the formation of electron holes in the perovskite sheets. Analogously, the introduction of transition metal cations with the average oxidation state higher than 2+ causes increasing oxygen interstitial concentration. Increasing the number of perovskite-type layers (n) leads to the formation of other RP nickelates (see, e.g. [14] and references therein); the end member with $n = \infty$ is perovskite-type $LaNiO_{3-\delta}$

* Corresponding author. Fax: +351 234 425300.
E-mail address: enaumovich@ua.pt (E.N. Naumovich).

0166-1280/$ - see front matter © 2009 Elsevier B.V. All rights reserved.
doi:10.1016/j.theochem.2009.12.003

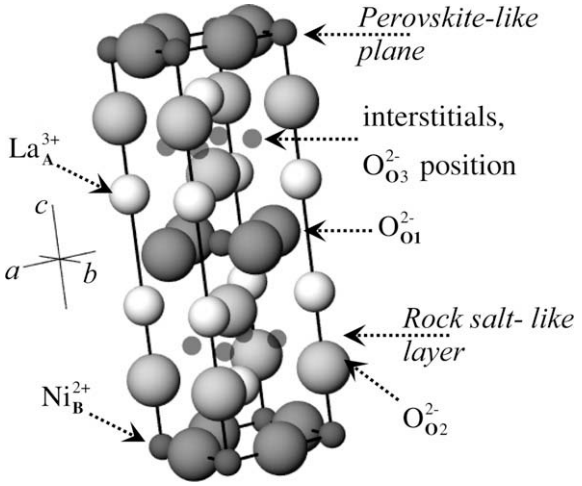

Fig. 1. Crystal structure of $La_2NiO_{4+\delta}$, comprising two regular oxygen sites (*O1* and *O2*) and interstitial *O3* positions. The subscripts *A* and *B* correspond to the general formula of K_2NiF_4-type oxide phases, A_2BO_4.

having a poor thermodynamic stability in the range of external conditions necessary for the practical applications.

One should separately note that the transitions between tetragonal and orthorhombic modifications of $La_2NiO_{4+\delta}$ [11,15–17] associated with the oxygen stoichiometry alterations occur mainly at relatively low temperatures, and have no essential effects on oxygen thermodynamics and high-temperature transport properties relevant for the electrochemical applications [9]. However, their possible influence on the SLS results cannot be *a priori* excluded, which made it necessary to assess local and global deviations from the tetragonal symmetry (space group *I4/mmm*) in the course of atomistic simulation studies.

Detailed description of the SLS and MD methods, and of the software used for modeling (GULP and DL_POLY 2, respectively), can be found in the literature [18–21]. Briefly, these calculations are based on the Born model for ionic solids; the charge of ions is considered equal to their formal oxidation state. The interactions between the ions are formulated in terms of long-range coulombic forces and two types of short-range interactions, namely the Pauli repulsion and van der Waals dispersion. The short-range forces are modeled using a standard Buckingham potential:

$$V_{ij} = A_{ij}\exp\left(-\frac{r}{\rho_{ij}}\right) - C_{ij}r^{-6} \quad (1)$$

where A_{ij}, ρ_{ij} and C_{ij} are the parameters related to ion–ion interactions, with the core–shell approach used to describe polarizability. The interatomic potentials used for the simulations are listed in Table 1. For the MD and SLS studies, the potential cutoff radii were selected equal to 18 Å and 16 Å, respectively. The simulation of all point defects was based on Mott–Littleton approach.

Table 1
Interatomic potentials used for the MD and SLS studies.

Ion	Buckingham			Core–shell			Ref.
	A (eV)	ρ (Å)	C (Å^{-6})	q_{core} (e)	q_{shell} (e)	k (Å^{-2})	
O^{2-}	22764.30	0.149	43.0	0.389	−2.389	42.0	[22]
La^{3+}	1545.213	0.35898	–	3.25	−0.25	145.0	[22]
$Ni^{(2+z)+}$	641.5	0.3372	–	$2+z$	n/a*	n/a	[23]
Fe^{3+}	1156.36	0.3299	–	4.97	−1.97	304.7	[24]
Co^{2+}	696.3	0.3362	–	2.0	n/a	n/a	[23]
Co^{3+}	1329.82	0.3087	–	0.96	2.04	196.3	[24]
Cu^{2+}	3799.3	0.2427	–	2	n/a	n/a	[25]

* n/a denotes that for this atoms simple core model was used.

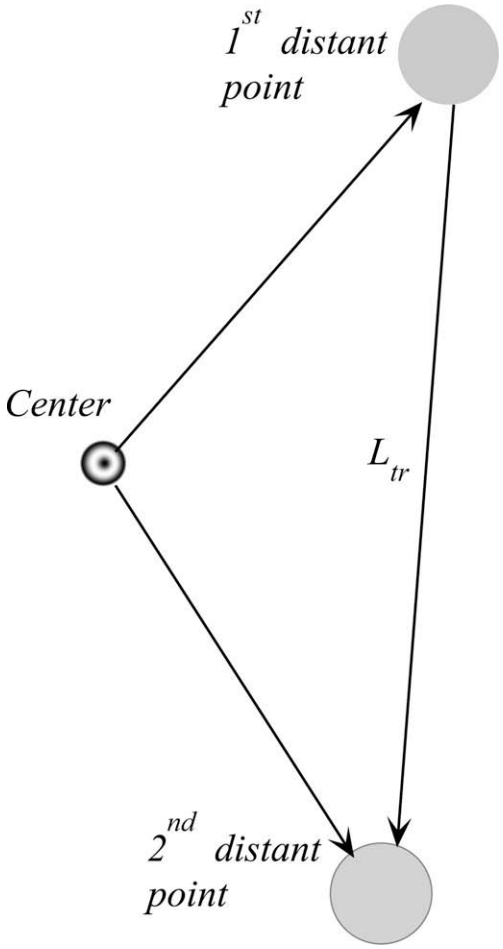

Fig. 2. Determination of the trajectory length L_{tr} (see text).

Table 2
Average coordination numbers and cation–anion distances, used to assign oxygen ions to the different sublattices after the course of MD simulations.

Oxygen positions	Neighborhood			
	Ni-site cations		La^{3+} cations	
	Average CN	Distance (Å)	Average CN	Distance (Å)
Immobile				
O1	1.9…2.1	0.1…3.0	0.0…0.1	0.5…2.2
O2	0.9…1.1	0.1…3.0	3.9…5.1	0.1…3.2
O3	0.0…0.1	0.1…3.0	2.9…4.1	0.1…3.2
O2n	0.9…1.1	0.1…3.0	2.9…5.1	0.1…3.2
Mobile				
O1m	1.0…2.1	0.1…3.0	0.0…0.1	0.5…2.2
O2m	0.9…1.1	0.1…3.0	2.9…5.1	0.1…3.2
O3m	0.0…0.1	0.1…3.0	1.9…4.1	0.1…3.2

Notes:
The symbol *O2n* corresponds to the *O2* sites with heavily distorted local neighborhood.
The *m* index corresponds to the mobile anions showed a non-negligible migration, $L_{tr} > 1.5$ Å.

Atomistic modeling of the oxidized $La_2NiO_{4+\delta}$-based lattices, where the δ values may be as high as 0.15–0.20, requires the use of a supercell approach. The supercell (SC) comprising a number of formula units is considered as primitive structural element, built on the basis of structural data. Such supercells with the size of

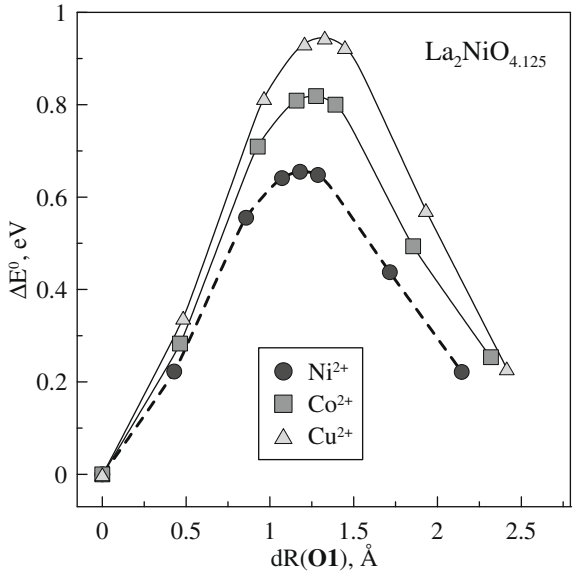

Fig. 3. Energy profile of the oxygen migration pathway near Ni^{2+}, Co^{2+} and Cu^{2+} cations in the perovskite-type layers of $La_2NiO_{4.125}$, calculated vs. initial anion position. dR is the distance from initial position.

$6 \times 6 \times 2$ and $4 \times 4 \times 1$ unit cells (~15.6 × 15.6 × 12.5 Å and ~22.8 × 22.8 × 25.6 Å, respectively) were used for SLS studies of ion migration in $La_2Ni(M)O_{4+\delta}$ (M = Fe, Co, Cu). The SC shape was chosen as close as possible to cubic in order to suppress artificial geometrical distortions. Taking into account the substantial delocalization of electron holes in La_2NiO_4-based phases [9], the charge of all nickel cations in the oxidized lattices was assumed to have an average value $(2 + z)$, $z \leqslant 0.25$, whereas the charge of Fe, Co and Cu cations was fixed at the values listed in Table 1. The corresponding potential constants (Table 1) were taken from Refs. [22–25]. In order to compare different compositions and to exclude effects of point-defect interactions on the parameters describing oxygen migration in the different lattices, the defect configurations neighboring a given mobile anion were always fixed equivalent for a given oxygen-nonstoichiometry value [26]. The lattice element with fixed point-defect configurations comprised, at least, one central and four neighboring NiO_6 or MO_6 octahedra and the relevant part of rock-salt type blocks; when placing this element in the SC, special care was taken to avoid presence of other oxygen interstitials (O_{i3}^{2-}) in the vicinity of the migrating anion. Notice that some asymmetry observed in the energy profiles of oxygen diffusion pathways, discussed below, is a result of local lattice distortions and influence of the distant point defects.

For the MD simulations, a series of SCs consisting of $12 \times 12 \times 4$ unit cells (~45.7 × 45.7 × 51.0 Å with >9000 atoms) with various anion and cation compositions were constructed. The simulation route included *npt hoover* lattice relaxation at a selected temperature for at least 100 ps to achieve stable SC geometry. The appropriate data may be easily collected from "STATIS" file [21] including time dependencies of the total pressure (p), temperature, cell volume (V), and mean squared displacements (MSD) for each kind of atoms; the stability of the SC geometry can be ascertained analyzing the variations of p, V and MSD for immobile atoms. Then *nve* simulation cycle was run to collect the ion migration data for at least 150 ps. No evidences of cation transport were found. During the *nve* simulations, the ion trajectories were recorded for, at least, 40–70 ps in the main course. For further treatment, the "HISTORY" file generated by the DL_POLY 2 software was converted to SQLite database [27], where the data were stored both as individual ion trajectories and as the lattice state at each step. The conversion enabled to conduct various type analyses of the trajectories. At the initial stage, the migrating species were detected calculating the characteristic trajectory length, L_{tr}. This route includes three steps shown schematically in Fig. 2:

(i) To calculate mean coordinates of the given ion in its trajectory ("*center*").
(ii) To find most distant point from the *trajectory center*.
(iii) To find the ion position most distant from both these points.

L_{tr} is the distance between the second and third positions, (ii) and (iii). This route was selected in order to avoid calculation issues originating from complicated shapes of the trajectories, such as cyclic. The minimum migration limit of 1.5 Å was used to separate *immobile* oxygen anions. The species with L_{tr} > 1.5 Å were then

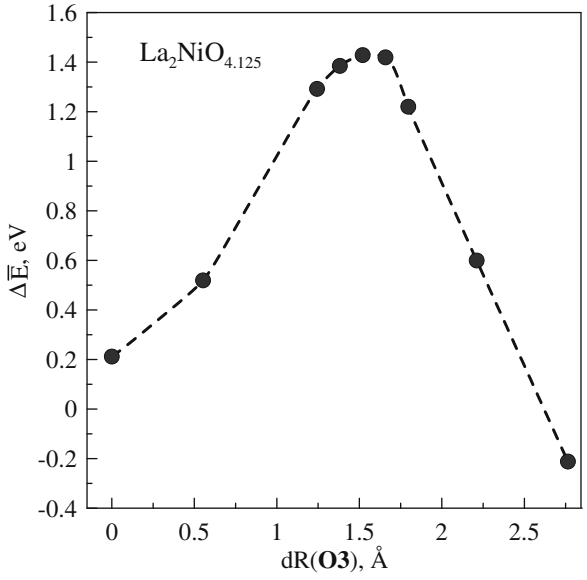

Fig. 4. Energy profile of the interstitial oxygen migration pathway in the rock-salt layer of $La_2NiO_{4.125}$, calculated vs. average energy of the initial and final positions.

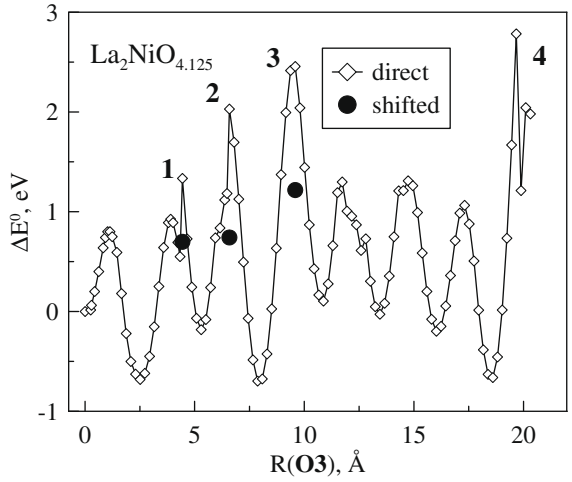

Fig. 5. Energy profile for direct migration of oxygen interstitial in the (1 1 0) direction. The marks 1,2 and 3 correspond to the saddlepoints (energy barrier peaks) in close proximity to another interstitial in the same rock-salt layer. For the point 3, two additional O_{i2}^{2-} interstitials are also present in the neighboring rock-salt layers. The point 4 corresponds to approaching another O_{i2}^{2-} anion in the trajectory line. The symbol • denotes peak energies in the points when small shift from linear trajectory occurs in the direction opposite to nearest-neighboring O_{i2}^{2-}.

considered as presumably mobile. The separation of all oxygen anions into two sorts, migrating and immobile, makes it possible to recover location of the migrated species with respect the different oxygen sublattices. Taking in account that at least ~8% ions should be considered as *presumably migrating* in the course of the calculations and $La_2NiO_{4+\delta}$ structure has 3 oxygen sublattices, this step was critical for further analysis. The nature of the MD data does not allow any exact assignment of the atoms to crystallographic positions due to thermal motion and long-range diffusion; however, it is possible to obtain information on the actual position of an oxygen anion in lattice by analyzing the population of its nearest-neighbor cations. In the case of *immobile* ions, the *trajectory centers* may be used for this purpose; for the migrating species, the analysis of nearest-neighboring cations along the whole trajectory is necessary. In latter case, the average coordination number (CN) should be used. Table 2 lists the characteristic ranges of CN and interatomic distances for the different oxygen sites. At the next stage of anion trajectory data analysis, the partial radial distribution functions (PRDFs) were analyzed. These were calculated in a manner similar to the corresponding DL_POLY procedure [21], but the central ions for each RDF were selected with respect to their sublattice and L_{tr} values. As a particular result, the role of local neighborhood on the anion diffusivity can be revealed. For solid solutions, relevant RDFs were normalized to the molar fraction of the species under consideration.

3. Results and discussion

3.1. Static lattice simulations

The oxygen ion transport in the perovskite-like layers of $La_2Ni(M)O_{4+\delta}$ can be described in terms of the vacancy migration mechanism well-known for the oxide perovskite phases [22,26]. In the case of K_2NiF_4-type nickelates, the vacancies existing in the perovskite-like sheets should indeed support a rather easy migration along the *a*–*b* plane. For instance, the migration energies calculated in the present work (Fig. 3) are similar or even lower than those for perovskite phases, namely ~0.8 eV when Co^{2+} is present in the

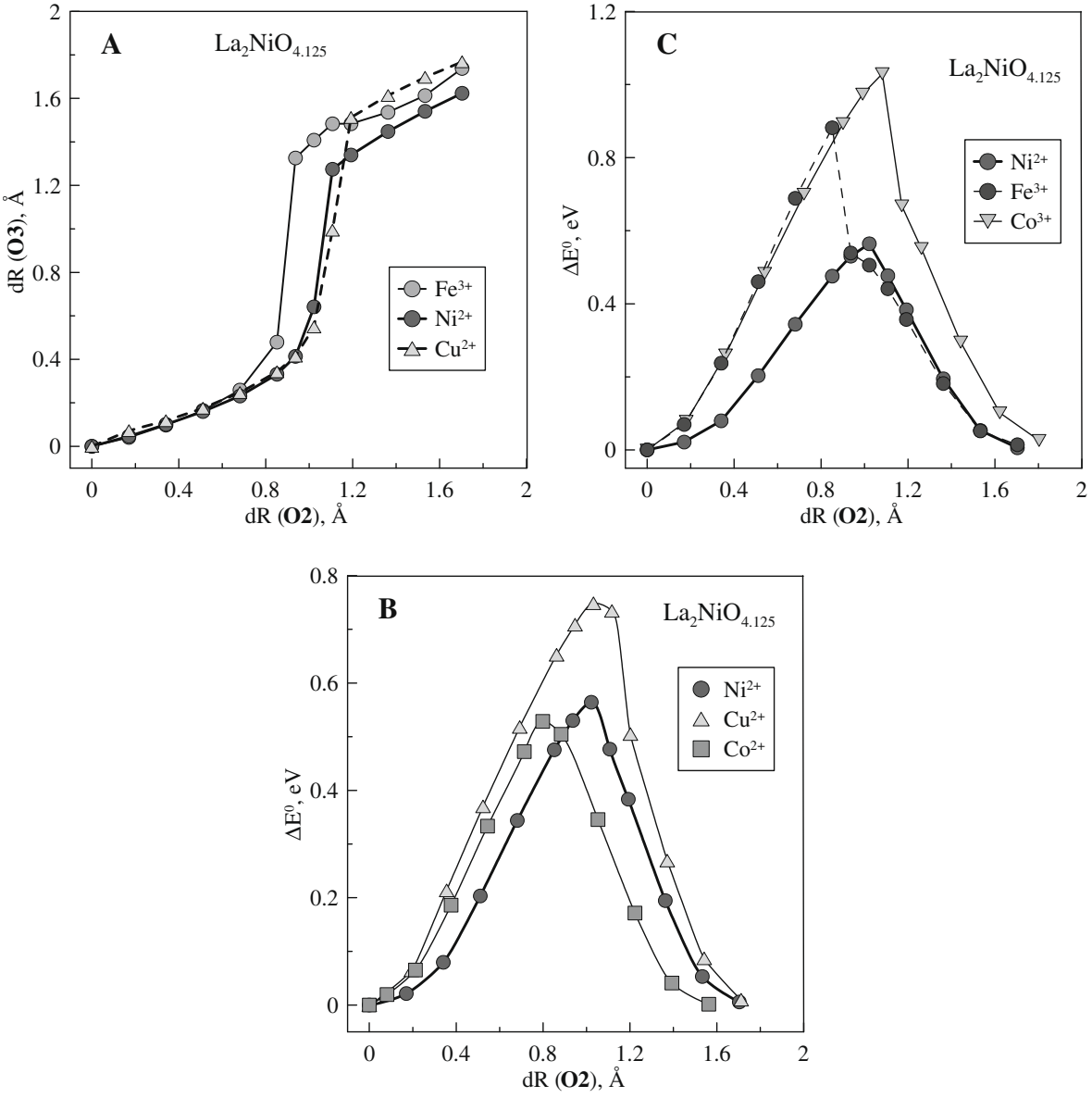

Fig. 6. Parameters describing the "dragging" migration mechanism in the rock-salt layer (see text): (A) cooperative migration diagram; (B and C) influence of the neighboring Ni-site cations on the energy profile.

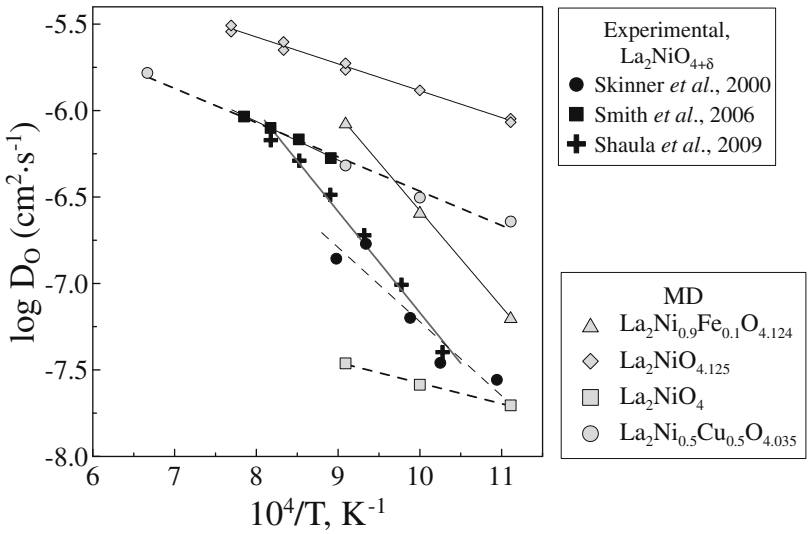

Fig. 7. Comparison of the oxygen diffusion coefficients in $La_2Ni(M)O_{4+\delta}$, calculated using MD technique, and literature data on $La_2NiO_{4+\delta}$ [10,29,30].

nearest neighborhood and <0.6 eV when the migrating anion is surrounded by Ni^{2+} only. However, our SLS results show that oxygen vacancies cannot exist near trivalent cations, such as Fe^{3+} or Co^{3+}, due to spontaneous reordering of oxygen-hyperstoichiometric $La_2Ni(M)O_{4+\delta}$ lattices. It should be separately mentioned that thermodynamic analysis of the $p(O_2)$-T-δ diagrams [28] displayed that the vacancy formation processes under thermodynamic equilibrium conditions are statistically insignificant in the case when $\delta \geqslant 0$. At the same time, statistical thermodynamic modeling makes it possible to only access the point-defect concentrations comparable to those of other lattice elements; the errors in the estimated concentrations of minor species is governed by the overall model errors. As discussed below, the present MD data confirm non-negligible oxygen migration in the perovskite layers of $La_2Ni(M)O_{4+\delta}$. The relevant mechanisms may be more complicated than those in perovskite-type oxides, involving cooperative movements of at least four oxygen ions. However, such simulations could not be performed by the SLS technique.

Nonetheless, atomistic modeling clearly demonstrated that simple anion jumps between the interstitial positions are associated with relatively high energetic barriers (Fig. 4). The corresponding pathways are quite long and asymmetric due to coulombic interactions between O_{O3}^{2-} ions. It should be mentioned that the calculated energetic barrier in the rock-salt layer (Fig. 4) is higher with respect to the interstitial migration activation energy for oxygen-stoichiometric La_2NiO_4 modeled by SLS, 0.77 eV [8], but is comparable to the barrier determined by the density functional theory (DFT) calculations for $La_2NiO_{4.125}$, ~1.2 eV [29]. This confirms, in particular, a critical impact of the extra oxygen concentration, whilst accounting for the electronic degrees of freedom via the use of DFT simulations of the rock-salt sheets with essentially ionic bonding seems less important. The latter statement is in agreement with the DFT results [29], which made it possible to rule out the charge transfer phenomena involving oxygen interstitials and electronic charge carriers. Another relevant conclusion is that, although simple anion jumps between the interstitial positions can still contribute to the substantially high ionic conductivity values [9,10], their major role seems unlikely. In this work, more prominent effects were found when an anion is "dragged" in the proximity to other interstitials (Fig. 5). This cooperative mechanism is based on the displacement of O_{O2}^{2-} due to the presence of nearest-neighboring O_{O3}^{2-} interstitials, and can be visualized by shifting an anion occupying the regular *O2* site in the direction from the nearest interstitial towards an empty interstitial position. As a result, after moderate displacement of "dragged" O_{O2}^{2-}, neighboring O_{O3}^{2-} jumps from interstitial into its position (Fig. 6A) and the migration pathway is substantially shortened (<2 Å for the cooperative mechanism vs. >2.5 Å for direct interstitial jumps). Furthermore, the resultant energetic barriers become significantly lower (Fig. 6). The substitution of nickel with dopant cations leads to a higher migration energy, as for the perovskite-type layer.

3.2. Molecular dynamics

The average oxygen diffusivity calculated from the MD data is in a reasonably good agreement with literature data [10,30,31], as illustrated by Fig. 7. In addition, the molecular dynamics analysis confirms important role of the trivalent dopant cations, such as Fe^{3+}, ascertained by the static lattice simulations. Namely, whilst increasing average cation charge increases the number of anionic charge carriers (interstitials), the presence of higher-valence cat-

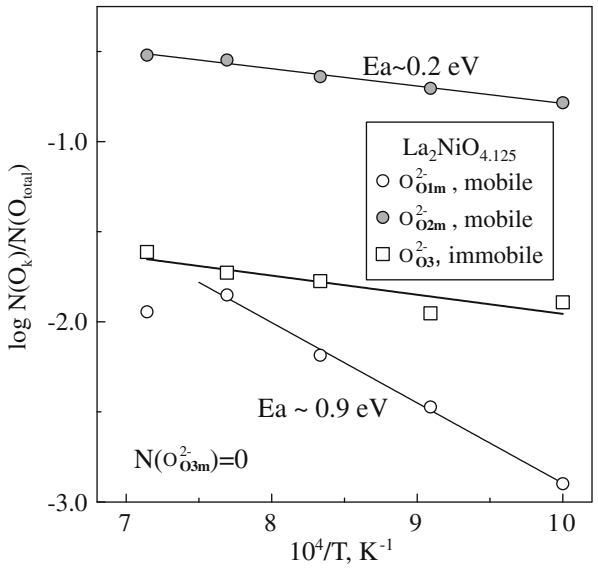

Fig. 8. Relative population of the mobile and immobile anions in the rock salt-type layers of $La_2NiO_{4.125}$, calculated from the MD results.

ions in the nickel sites was found to suppress anion migration in near neighborhood. Note that stoichiometric La_2NiO_4 displays a relatively low, but non-negligible oxygen diffusivity.

The analysis of microscopic ion-migration data in combination with the initial positions of anions enables to understand more detailed mechanisms (Fig. 8). In the case of substantially oxidized $La_2NiO_{4.125}$, main contribution to the ionic transport is provided by the *O2* sites. The activation energy characteristic for this sublattice, calculated from temperature dependencies of the oxygen diffusion coefficients, is as low as ~0.2 eV. More interesting is that no direct migration between the interstitial *O3* positions was detected, thus providing an additional argument in favor of the "dragging" mechanism suggested on the basis of static-lattice simulations. Furthermore, the apparent activation energy for the oxygen anion diffusion mechanism involving equatorial sites in the perovskite-type layers, which comprises the defect formation energy-related contributions, is considerably higher compared to the cooperative mechanisms involving rock-salt sheets. This difference explains well the deviations from Arrhenius behavior, observed experimentally for the oxygen ionic conduction and anion mobility in $La_2NiO_{4+\delta}$-based phases where the apparent activation energy tends to increase when temperature decreases [2,9,10,32]. Such a tendency can be illustrated by the oxygen diffusion coefficients calculated from the oxygen permeation fluxes through dense $La_2NiO_{4+\delta}$ membranes [10], as shown in Fig. 7; the activation energy is 0.78 eV at 1173–1223 K and increases up to 1.2–1.5 eV on cooling. This increase is primarily associated with decreasing number of mobile *O1* ions and, therefore, vacancies in the equatorial sites, thus increasing two-dimensional character of the anion migration. The SLS data discussed above show that the incorporation of higher-valence dopants, such as Co^{3+} and Fe^{3+}, should promote these effects. In combination with rising energetic barriers in the rock-salt layers (Fig. 6C), the modeling results clarify also the higher activation energy for ionic transport, characteristic of Co- and Fe-substituted nickelates in the intermediate-temperature range [9,32]. Moreover, if the hypothesis concerning relationships between the vacancy-formation and anion-migration processes in the perovskite-type layers of $La_2Ni(M)O_{4+\delta}$ and surface exchange kinetics [9,10] is correct, the MD data may explain why the activation energy for surface exchange is higher than that for the bulk ionic transport. The calculated anion diffusion pathways in the rock-salt and perovskite-type layers are illustrated by Fig. 9.

Consideration of the calculated RDFs shows that all Fe^{3+} cations incorporated in the lattice remain hexa-coordinated, whereas the average CNs of nickel tends to vary due to the diffusion of oxygen occupying *O2* sites. The *O1* sites near nickel cations remain completely filled with oxygen. These results may indicate likely origin of the decrease in O^{2-}_{O2} concentration when temperature increases at $\delta = const$ (Fig. 8). The *O2* sublattice becomes more and more disordered on heating; a part of the oxygen anions occupying *O2* sites at low temperatures move towards interstitial sites.

Fig. 10 illustrates the critical impact of incorporated Fe^{3+} cations, which act as *anion traps* and impede long-range migration (L_{tr} > 3.0 Å) of the neighboring oxygen. The observed effects of cop-

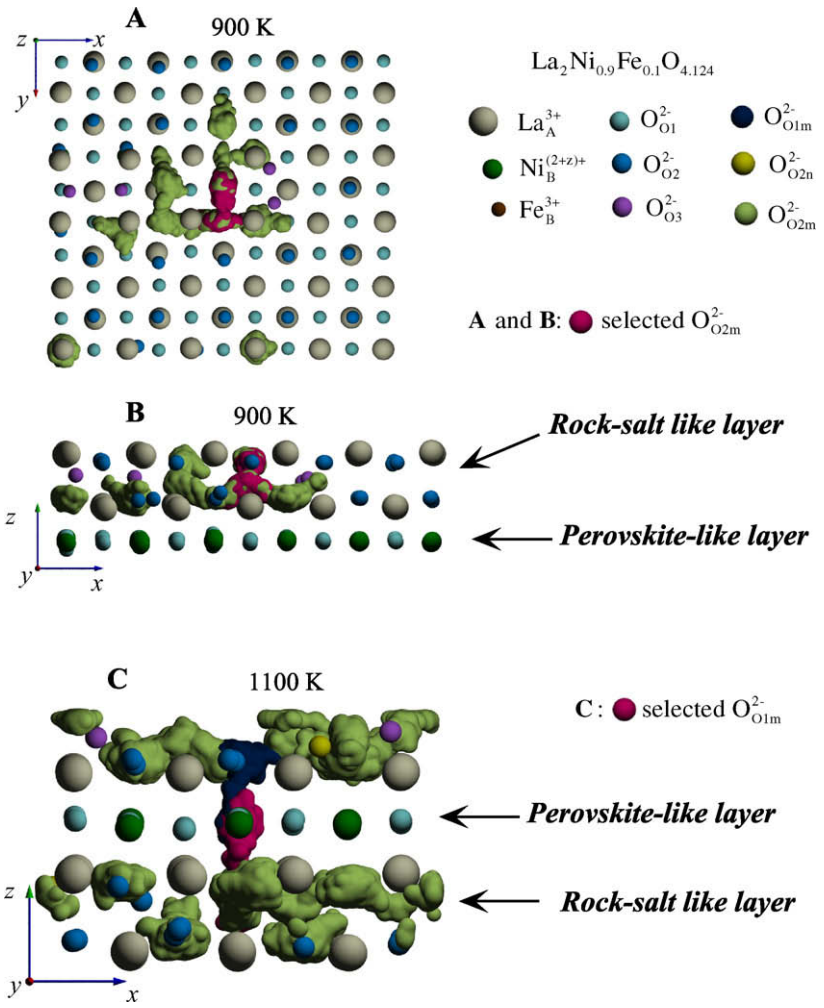

Fig. 9. Examples of the oxygen migration pathways in $La_2Ni_{0.9}Fe_{0.1}O_{4.124}$ during 50 ps. Immobile species are presented as single spheres at their averaged positions. The mobile anions are shown as sequence of their position along the corresponding trajectories with 0.01 ps step. The axes length corresponds to 3 Å.

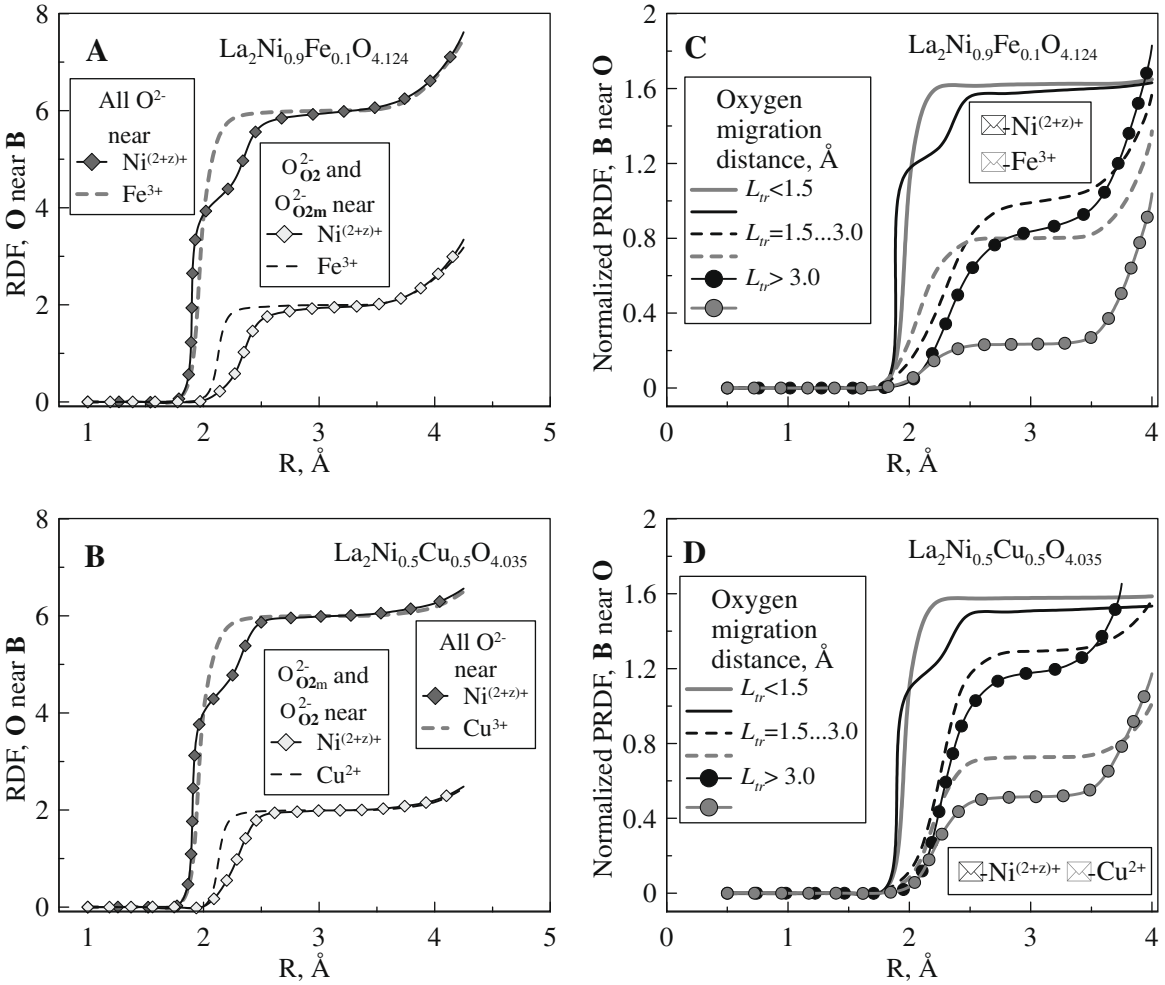

Fig. 10. Partial radial distribution functions in $La_2Ni_{0.9}Fe_{0.1}O_{4+\delta}$ and $La_2Ni_{0.5}Cu_{0.5}O_{4+\delta}$ at 1100 K: (A and B) Oxygen near Ni-site cations, (C and D) Ni-site cations near oxygen.

per doping on the oxygen mobility are also in agreement with SLS results. However, whilst Cu^{2+} tends to slightly suppress anion diffusion, no *trapping* phenomena can be identified (Fig. 10C). This suggests that oxygen trapping near Fe^{3+} may be attributed mainly to the coulombic forces.

4. Conclusions

The computer simulation studies of mixed-conducting $La_2Ni(M)O_{4+\delta}$ (M = Fe, Co, Cu), including both static lattice and molecular dynamics (MD) methods, were used to analyze microscopic anion-diffusion mechanisms having a primary importance for applications of these materials. Emphasis was given to the identification of likely anion-migration pathways, relevant energetic parameters and effects of the transition metal cation dopants. The actual initial positions of anions occupying different oxygen positions in the K_2NiF_4-type structure of $La_2Ni(M)O_{4+\delta}$, were determined from the MD data. The corresponding effects on ionic mobility were appraised. It was shown that while the substitution of Ni^{2+} with higher-valence cations leads to a higher ionic charge-carrier concentration, such dopants tend to decrease mobility of the oxygen anions, both in the rock-salt and perovskite-like layers of the K_2NiF_4-type structure. The most likely mechanisms of anion diffusion in oxygen-hyperstoichiometric $La_2Ni(M)O_{4+\delta}$ include the O_{O2}^{2-}–O_{O3}^{2-} exchange in the rock-salt type sheets and cooperative transport across the perovskite layer, all involving several ionic species.

Acknowledgements

This work was partially supported by the FCT, Portugal (projects POCI/CTM/59197/ 2004 and PTDC/CTM/64357/2006).

References

[1] B. Vigeland, R. Glenne, T. Breivik, S. Julsrud, Int. Patent Application PCT WO 99/59702 (1999).
[2] V.V. Kharton, A.P. Viskup, E.N. Naumovich, F.M.B. Marques, J. Mater. Chem. 9 (1999) 2623.
[3] V.V. Vashook, N.E. Trofimenko, H. Ullmann, L.V. Makhnach, Solid State Ionics 131 (2000) 329.
[4] D.C. Zhu, X.Y. Xu, S.J. Feng, W. Liu, C.S. Chen, Catal. Today 82 (2003) 151.
[5] V.V. Kharton, A.V. Kovalevsky, M. Avdeev, E.V. Tsipis, M.V. Patrakeev, A.A. Yaremchenko, E.N. Naumovich, J.R. Frade, Chem. Mater. 19 (2007) 2027–2033.
[6] S.J. Skinner, J.A. Kilner, Ionics 5 (1999) 171.
[7] L. Minervini, R.W. Grimes, J.A. Kilner, K.E. Sickafus, J. Mater. Chem. 10 (2000) 2349.
[8] A.R. Cleave, J.A. Kilner, S.J. Skinner, S.T. Murphy, R.W. Grimes, Solid State Ionics 179 (2008) 823.
[9] V.V. Kharton, E.V. Tsipis, E.N. Naumovich, A. Thursfield, M.V. Patrakeev, V.A. Kolotygin, J.C. Waerenborgh, I.S. Metcalfe, J. Solid State Chem. 181 (2008) 1425–1433.
[10] A.L. Shaula, E.N. Naumovich, A.P. Viskup, V.V. Pankov, A.V. Kovalevsky, V.V. Kharton, Solid State Ionics 180 (2009) 812–816.
[11] J. Rodríguez-Carvajal, M.T. Fernández-Díaz, J.L. Martínez, J. Phys. Condens. Matter 3 (1991) 3215.
[12] M. Hücker, K. Chung, M. Chand, T. Vogt, J.M. Tranquada, D.J. Buttrey, Phys. Rev. B 70 (2004) 064105.
[13] H. Tamura, A. Hayashi, Y. Ueda, Physica C 258 (1996) 61.
[14] G. Amow, I.J. Davidson, S.J. Skinner, Solid State Ionics 177 (2006) 1205.
[15] S.J. Skinner, Solid State Sci. 5 (2003) 419–426.

[16] W. Paulus, A. Cousson, G. Dhalenne, J. Berthon, A. Revcolevschi, S. Hosoya, W. Treutmann, G. Heger, R. Le Toquin, Solid State Sci. 4 (2002) 565–573.
[17] H.L. Zhang, X.S. Wu, C.S. Chen, W. Liu, Phys. Rev. B 71 (2005) 064422.
[18] J.D. Gale, J. Chem. Soc., Faraday Trans. 93 (1997) 629.
[19] J.D. Gale, A.L. Rohl, Mol. Simul. 29 (2003) 291.
[20] W. Smith, T.R. Forester, J. Mol. Graph. 14 (1996) 136.
[21] W. Smith, T.R. Forester, I.T. Todorov, The DL_POLY_2.0 User Manual, Daresbury Laboratory, United Kingdom, 2009.
[22] M.S. Khan, M.S. Islam, D.R. Bates, J. Phys. Chem. B 102 (1998) 1099.
[23] V. Lewis, C.R.A. Catlow, J. Phys. C: Solid State Phys. 18 (1985) 1149.
[24] M. Cherry, M.S. Islam, C.R.A. Catlow, J. Solid State Chem. 118 (1995) 25.
[25] M.S.D. Read, M.S. Islam, G. Watson, F. King, F.E. Hancock, J. Mater. Chem. 10 (2000) 2298.
[26] E.N. Naumovich, M.V. Patrakeev, V.V. Kharton, M.S. Islam, A.A. Yaremchenko, J.R. Frade, F.M.B. Marques, Solid State Ionics 177 (2006) 457–470.
[27] http://www.sqlite.org/.
[28] E.N. Naumovich, M.V. Patrakeev, V.V. Kharton, A.A. Yaremchenko, D.I. Logvinovich, F.M.B. Marques, Solid State Sci. 7 (2005) 1353–1362.
[29] C. Frayret, A. Villesuzanne, M. Pouchard, Chem. Mater. 17 (2005) 6538.
[30] S.J. Skinner, J.A. Kilner, Solid State Ionics 135 (2000) 709.
[31] J.B. Smith, T. Norby, J. Electrochem. Soc. 153 (2006) A233.
[32] V.V. Kharton, A.P. Viskup, A.V. Kovalevsky, E.N. Naumovich, F.M.B. Marques, Solid State Ionics 143 (2001) 337.